SCIENTIFIC REPORTS
nature research

OPEN

The neuronal ceroid lipofuscinosis protein Cln7 functions in the postsynaptic cell to regulate synapse development

Kyle J. Connolly[1,5], Megan B. O'Hare[2,5], Alamin Mohammed[1,5], Katelyn M. Aitchison[1], Niki C. Anthoney[1], Matthew J. Taylor[1], Bryan A. Stewart[3,4], Richard I. Tuxworth[1,6*] & Guy Tear[2,6*]

The neuronal ceroid lipofuscinoses (NCLs) are a group of fatal, monogenic neurodegenerative disorders with an early onset in infancy or childhood. Despite identification of the genes disrupted in each form of the disease, their normal cellular role and how their deficits lead to disease pathology is not fully understood. Cln7, a major facilitator superfamily domain-containing protein, is affected in a late infantile-onset form of NCL. Cln7 is conserved across species suggesting a common function. Here we demonstrate that Cln7 is required for the normal growth of synapses at the *Drosophila* larval neuromuscular junction. In a *Cln7* mutant, synapses fail to develop fully leading to reduced function and behavioral changes with dysregulation of TOR activity. *Cln7* expression is restricted to the post-synaptic cell and the protein localizes to vesicles immediately adjacent to the post-synaptic membrane. Our data suggest an involvement for Cln7 in regulating trans-synaptic communication necessary for normal synapse development.

The study of early-onset, inherited forms of neurodegenerative disease provides an opportunity to identify how single gene defects lead to neurodegeneration. The neuronal ceroid lipofuscinoses (NCLs) are a group of such monogenetic neurodegenerative disorders with disease onset early in infancy or childhood (5–8 years in the most common form but congenital and rare adult-onset forms also exist). Patients present with a loss of visual acuity followed by onset of seizures and psychiatric disturbances. A progressive mental decline follows, accompanied by loss of motor skills and death usually occurs by the age of 20–30[1]. The progression of NCL pathology appears similar to many other neurodegenerative disorders in that changes to synapses occur very early and a local activation of glia precedes a regionally specific loss of neurons[2,3].

The NCLs are recessively inherited monogenic disorders (with the exception of one rare adult-onset autosomal dominant form) and mutations have been identified in 13 genes responsible for NCL with varying ages of onset. Mutations in *CLN7/MFS domain-containing 8* (*CLN7*/*MFSD8*) are responsible for late-infantile onset NCL (LINCL or CLN7 disease), with disease onset at 1.5–5 years of age[4]. The CLN7 protein is predicted to be a member of the major facilitator superfamily of transporters, the majority of which have twelve membrane spanning domains[5]. In cell culture experiments with tagged forms, CLN7 protein is localized primarily in lysosomes[5–7] and has been identified by lysosomal proteomics[8]. Mouse embryonic fibroblasts derived from *CLN7* deficient mice show a loss of lysosomal proteins and deficits in mTOR reactivation[9]. In the mouse retina, CLN7 protein co-localizes with the post-synaptic density marker, PSD-95[10], indicating the potential for alternative localization in specialist cells.

The *in vivo* function of Cln7 remains unknown. Mutant mice show lysosomal dysfunction and a potential impairment of autophagy[11] but it is unclear how this leads to neurodegeneration. Evidence is building that loss

[1]Institute of Cancer and Genomic Sciences, University of Birmingham, Birmingham, B15 2TT, UK. [2]Department of Developmental Neurobiology, King's College London, New Hunt's House, London, SE1 1UL, UK. [3]Department of Biology, University of Toronto Mississauga, Mississauga, ON, L5L 1C6, Canada. [4]Department of Cell and Systems Biology, University of Toronto, Toronto, ON, M5S 3G5, Canada. [5]These authors contributed equally: Kyle J. Connolly, Megan B. O'Hare and Alamin Mohammed. [6]These authors jointly supervised this work: Richard I. Tuxworth and Guy Tear. *email: R.I.Tuxworth@bham.ac.uk; Guy.Tear@kcl.ac.uk

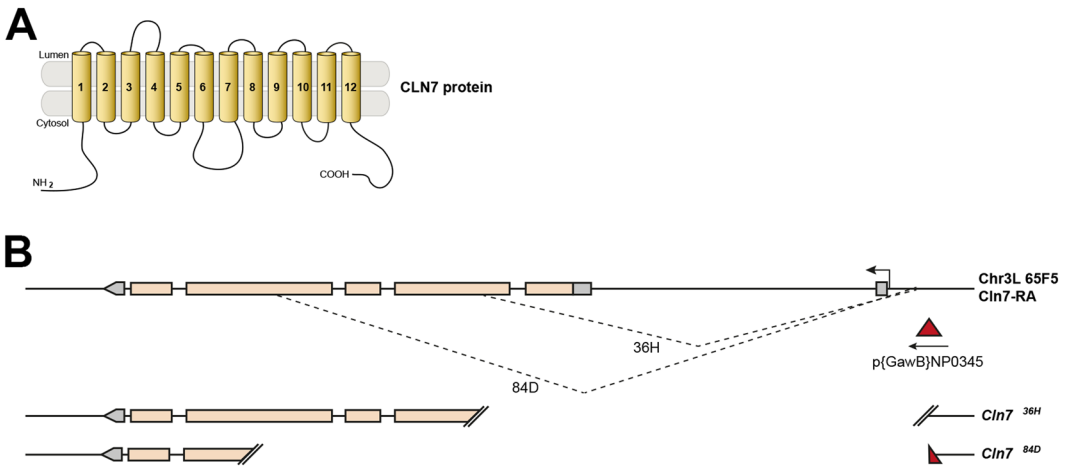

Figure 1. Generation of *Cln7* mutations. (**A**) Cln7 is predicted to be a 12-span transmembrane protein and member of the multifacilitator superfamily of solute transporters. (**B**) P-element-mediated imprecise excision was used to generate deletions within the *Cln7* locus (CG8596). Two unidirectional deletion events, 36H and 84D, are shown diagrammatically. Some of the P-element sequence is retained in the *84D* allele.

of the *CLN* genes impacts on synapse function, suggesting that they play a common role either within neurons or non-neuronal cells in the development or homeostasis of synapses[2,12,13]. To further investigate potential roles for Cln7 we have made use of *Drosophila* where many genes associated with human neurological conditions, including developmental disorders and neurodegenerative diseases, have been identified to have conserved roles[7,14]. *Drosophila* has one clear orthologue of *Cln7*[15], which is widely expressed both in the CNS and other tissues[16]. Similarly to the mammalian form, the *Drosophila* Cln7 protein localizes to lysosomes and but also has prominent localization at the plasma membrane[16]. We have investigated the role of Cln7 at the *Drosophila* neuromuscular junction (NMJ), a model glutaminergic synapse which provides a simple, genetically tractable system to study the core processes of synapse assembly and homeostasis[17]. The NMJ exhibits both short-term and longer-term homeostasis mediated by multiple cellular pathways, acting at both sides of the synapse, and many of these mechanisms also act similarly to regulate homeostasis in mammalian neurons[18]. In addition, normal autophagic flux and endo-lysosomal function are known to maintain the synapse. Mutants affecting lysosomal function or autophagy, including *spinster* and the cation channel *Trpml*, impact on NMJ development and cause expansion of the synapse[19–21]. Neural expression of *Drosophila Cln7* is largely restricted to the optic system but it is expressed more widely in the CNS in glia, including in the glia that form the blood-brain-barrier and in the ensheathing glia that wrap axons[16]. *Cln7* is also expressed in the neuromuscular system where high levels are found in the muscles which form the postsynaptic cell of the NMJ.

To study Cln7 requirement *in vivo*, we generated a *Drosophila* model for CLN7 disease by deleting the N-terminal half of the *Cln7* gene. While the animals remain viable, they display impaired locomotion and an associated reduction in synapse size and altered synapse function. We show that a population of Cln7-containing vesicles localizes at the post-synaptic side of the synapse but autophagy is largely intact in the *cln7* mutants and retrograde BMP signaling pathway driving pre-synapse growth functions normally. We show that there is a molecular interaction between Cln7 and the TOR complex activator, Rheb, which suggests Cln7 regulates neural development via TOR from a post-synaptic vesicular compartment.

Results

Generation of a *Drosophila* model of CLN7 disease. Disruption of the *MFSD8/CLN7* gene has been identified as the cause of the LINCL form of the NCLs[4]. Subsequently, more than 30 different *Cln7* mutations have been characterized. The *Drosophila* gene CG8596 shows 57% amino acid homology to human *CLN7* and is the unique *Drosophila* orthologue of *Cln7*[15,22]. The gene encodes a predicted 12-spanning transmembrane protein that has strong sequence homology to the multifacilitator family of solute transporters (Fig. 1A)[15]. In a parallel study we generated Venus-YFP knock-in forms of Cln7 by CRISPR/Cas9-mediated gene editing to act as a reporter of expression and sub-cellular localization[16]. *Cln7* is predominantly a glial protein in the *Drosophila* CNS but it is also expressed in the neurons of the visual system, starting during the early stages of eye development in the late larva and persisting in adult flies (Supplemental Fig. S1) and consistent with the visual pathology that manifests early in CLN7 disease[16]. To study the functional role of Cln7, we generated two loss-of-function alleles of *Cln7* by imprecise excision of the P-element, NP0345, that is inserted in the upstream region proximal to the start codon (Fig. 1B). Two alleles were generated. Exons 1–5 were excised with some P-element sequence remaining in the $Cln7^{84D}$ allele, and exons 1 and 2 and part of exon 3 were excised in the $Cln7^{36H}$ allele (Fig. 1B). Both mutant alleles are viable and fertile when homozygous.

Cln7 is localized to the post-synaptic side of the neuromuscular junction. As there is growing speculation that the synapse is a target of disease in the NCLs, we investigated whether Cln7 functions at the *Drosophila* neuromuscular junction (NMJ), a model glutamatergic synapse that is routinely used to gain insight

into molecular function of proteins associated with human neurological disease[14]. Using a YFP-Cln7 knock-in reporter line we find *Cln7* is expressed in the glia that ensheath the motor neurons and also in the body wall muscles that form the post-synaptic cells of the NMJ[16]. The expression levels of the YFP reporter are low, as might be expected for the endogenous levels of Cln7. We further examined the localization of Cln7 using higher-resolution Airyscan confocal imaging. We find that Cln7 is present in puncta throughout the muscle cell but also concentrates at the post-synaptic site (Fig. 2A). Surrounding each pre-synaptic swelling (or bouton) is a convoluted membranous structure known as the sub-synaptic reticulum (SSR), which contains the post-synaptic glutamate receptors. A commonly-used marker of the SSR, anti-Discs large (Dlg, the *Drosophila* PSD-95 ortholog), appears in a continuous pattern around the boutons but higher-resolution imaging reveals that Cln7 is clearly localized to discrete vesicles immediately surrounding the post-synaptic site, rather than in the plasma membrane of the cell (Fig. 2B). The nature of the Cln7-containing vesicles is not clear but they do not appear to contain Cathepsin L, a lysosomal marker, and lysosomes do not concentrate at the synapse (not shown).

Localization of some proteins to the SSR, such as Coracle, requires staufen-dependent trafficking of the mRNA and local translation[23]. Cln7 and Coracle proteins are both concentrated at the post-synaptic site and are also both expressed in the ensheathing glia that wrap the motor axons (Fig. 2D). However, Cln7 localization is not likely to require local translation at the post-synaptic site because localization is maintained even when a N-terminally-tagged Cln7 fusion protein (Myc-BioID-Cln7) is overexpressed under the control of Mef2-Gal4 and with the endogenous *Cln7* 3′UTR absent (Fig. 2C).

Cln7 is required for normal synaptic growth. The distribution of Cln7 within post-synaptic vesicles suggests the protein may function to regulate the synapse and, since LINCL may be a result of synapse failure, we investigated the consequence of a loss of *Cln7* function. The *Drosophila* NMJ is a readily accessible glutamatergic synapse and an excellent model system to study synapse function[17], so this discovery afforded us an opportunity to ask how Cln7 might function at the post-synaptic site. The peripheral NMJs in late-stage larvae are easily identifiable using immunofluorescence and the innervations are simple, with 2–4 individual motoneurons contacting each muscle cell. The type I motoneurons that innervate the muscle can be further subdivided into two classes called type Ib and type Is classified according to the size of the presynaptic terminal swellings, known as boutons (Fig. 3A). The type Ib terminals provide tonic stimulation and the type Is phasic[24]. The overall size of the NMJ is governed by intra-neuronal and trans-synaptic homeostatic mechanisms that modulate NMJ size during development to match pre-synapse size and strength to muscle size[18]. Many mutations affecting the structural and electrical properties of the NMJ consequently affect its size at the late larval stage, including many mutations related to human neurological diseases[14].

We find that in $Cln7^{-/-}$ animals the NMJ is reduced in size. Manual counting of the swellings of the terminal (boutons) is commonly used as a simple measure of terminal size as the boutons contain most of the active zone synaptic vesicle release sites. At muscle 4 we see a significant reduction of the type Ib motoneuron terminals in the *Cln7* mutant larvae when compared to isogenic control larvae (Fig. 3A). This reduction is consistent with a reduction in synapse growth rather than degeneration as staining with anti-Dlg fails to reveal remnants of postsynaptic specializations left after neuron retraction (data not shown). Some of the boutons in the *Cln7* larvae appeared larger so we also used a non-subjective method of measuring terminal volume from 3D-rendered confocal images. Again, the type Ib terminals were significantly smaller than controls but, interestingly, the type Is terminals were unaffected (Fig. 3B). As a further measure of synapse size, we counted the number of active zones at the NMJ. Active zones are visualized with an antibody to Bruchpilot (ELKS), an active zone component[25]. Bruchpilot positive puncta were counted at muscle 4 and this confirmed that the number of active zones within Ib boutons is reduced in $Cln7^{-/-}$ animals concomitant with the reduction in volume but is unchanged in type Is junctions (Fig. 3C). Both alleles of *Cln7* had an identical phenotype as does the transheterozygous combination. Interestingly, both alleles were also haploinsufficient, suggesting some processes important for NMJ development are critically dependent on the levels of the *Cln7* protein. These results suggest a requirement for Cln7 for normal synapse development.

Cln7 function is required in the post-synaptic side of the NMJ. To investigate whether Cln7 is required in the post synaptic cell we used RNAi to reduce *Cln7* expression in various cell types at the synapse. Standard GAL4 drivers were used to express dsRNA specifically targeted at *Cln7* either pre-synaptically (Elav-Gal4), post-synaptically in the muscle (Mef2-Gal4), in all glia (Repo-Gal4) and in only the perineurial glia (PG-Gal4) that form the blood-brain-barrier, where *Cln7* is also highly expressed[16]. Only knockdown of *Cln7* in the muscle replicated the under-development phenotype at the NMJ (Fig. 3D), consistent with the expression of *Cln7*. We also performed the converse experiment of re-expressing YFP-Cln7 in the $Cln7^{-/-}$ background, again with ubiquitous expression (actin-Gal4) or expression restricted to neurons (Elav-Gal4), to muscle (Mef2-Gal4), in both neurons and muscle together (Spin-Gal4) or to glia (Repo-Gal4). Muscle expression with Mef2- or Spin-Gal4 was only capable of partial rescue of function which narrowly failed to reach significance. Only ubiquitous expression fully rescued the phenotype (Fig. 3E) indicating that some Cln7 function is required elsewhere in addition to the muscle.

Loss of Cln7 leads to synapse dysfunction. To examine the consequence of the abnormal synaptic growth we characterized synaptic physiology and larval motility. An electrophysiological analysis of the NMJ was carried out using intracellular recordings. We recorded the spontaneous transmitter release at the larval NMJs for two minutes to calculate miniature excitatory junction potential (mEJP) frequency and amplitude in 0.5, 0.75, 1.0 and 2.0 mM extracellular Ca^{2+} concentration but there was no significant difference due to genotype in either case (Fig. 4A; 2-way ANOVA with Sidak's multiple comparison test, $p = 0.483$). Taken together, we concluded there was likely to be little overt change in spontaneous synaptic vesicle release or post-synaptic receptor density.

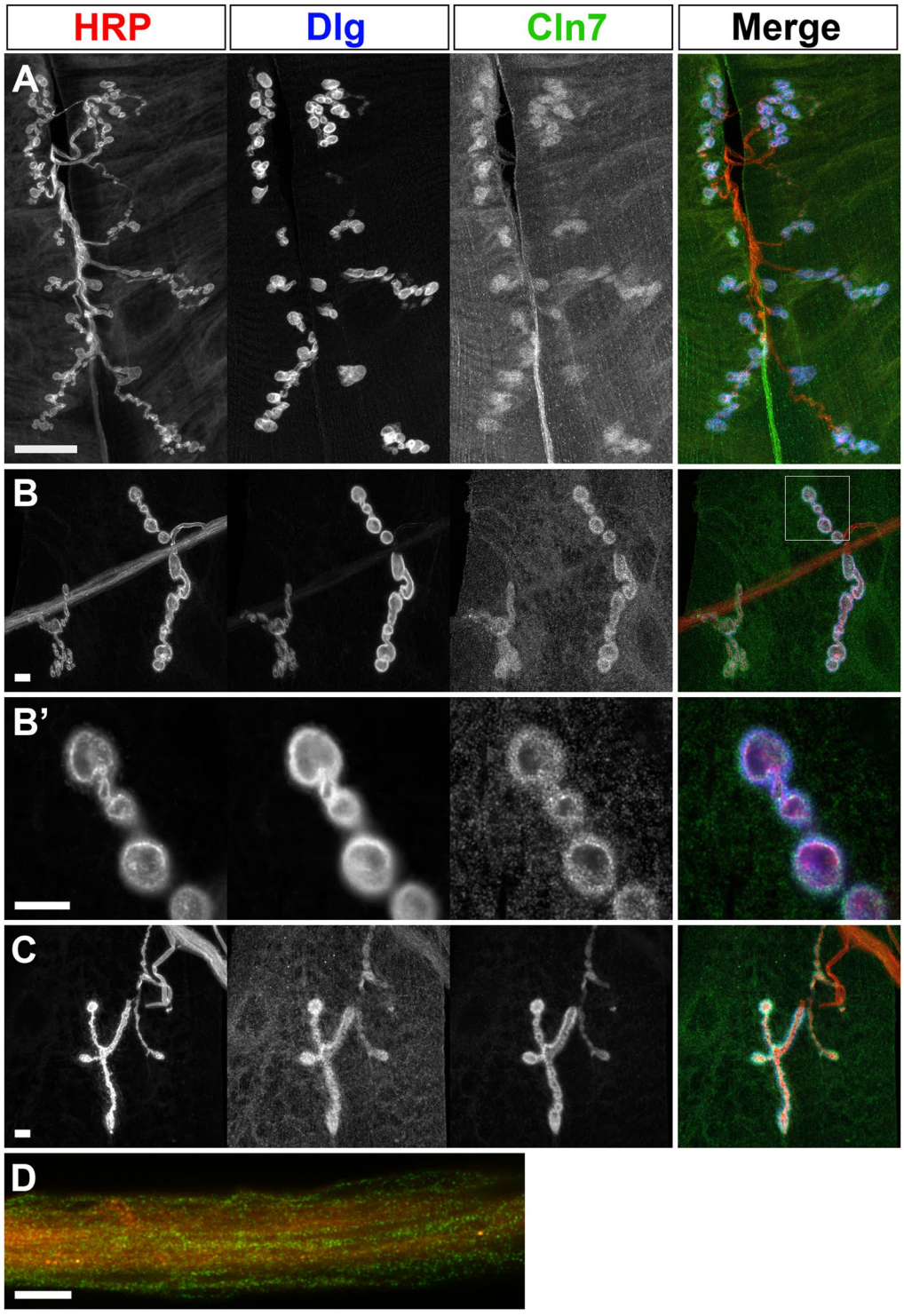

Figure 2. Cln7 localizes to a vesicular compartment at the post-synaptic membrane. (**A,B**) Late larval NMJs from a YFP-Cln7 knock-in reporter line fixed and stained for the neuronal plasma membrane (anti-HRP, red), the sub-synaptic reticulum membrane (anti-Dlg, blue) and for YFP-Cln7 (anti-GFP, green). YFP-Cln7 is restricted to the post-synaptic muscle cell at the larval neuromuscular junction. (**A**) Show NMJ6-7 and (**B**) shows NMJ4b. The boxed region in B was imaged at higher resolution in B'. Distinct $Cln7^{+}$ vesicles are concentrated within and around the sub-synaptic reticulum. (**C**) A Myc-BioID-Cln7 fusion protein is still recruited to the sub-synaptic reticulum when overexpressed from a cDNA construct in the muscle lacking the endogenous 3'UTR. Anti-Myc (green) was used to visualize the Cln7 fusion. (**D**) YFP-Cln7 is also expressed in the ensheathing glia that wrap axons in the nerves. Transverse optical section through intersegmental nerve 1b stained with anti-HRP (neurons, red) anti-GFP (YFP-Cln7, green). Bar = 10 μm (**A**,**D**); 5 μm (**B**,**C**).

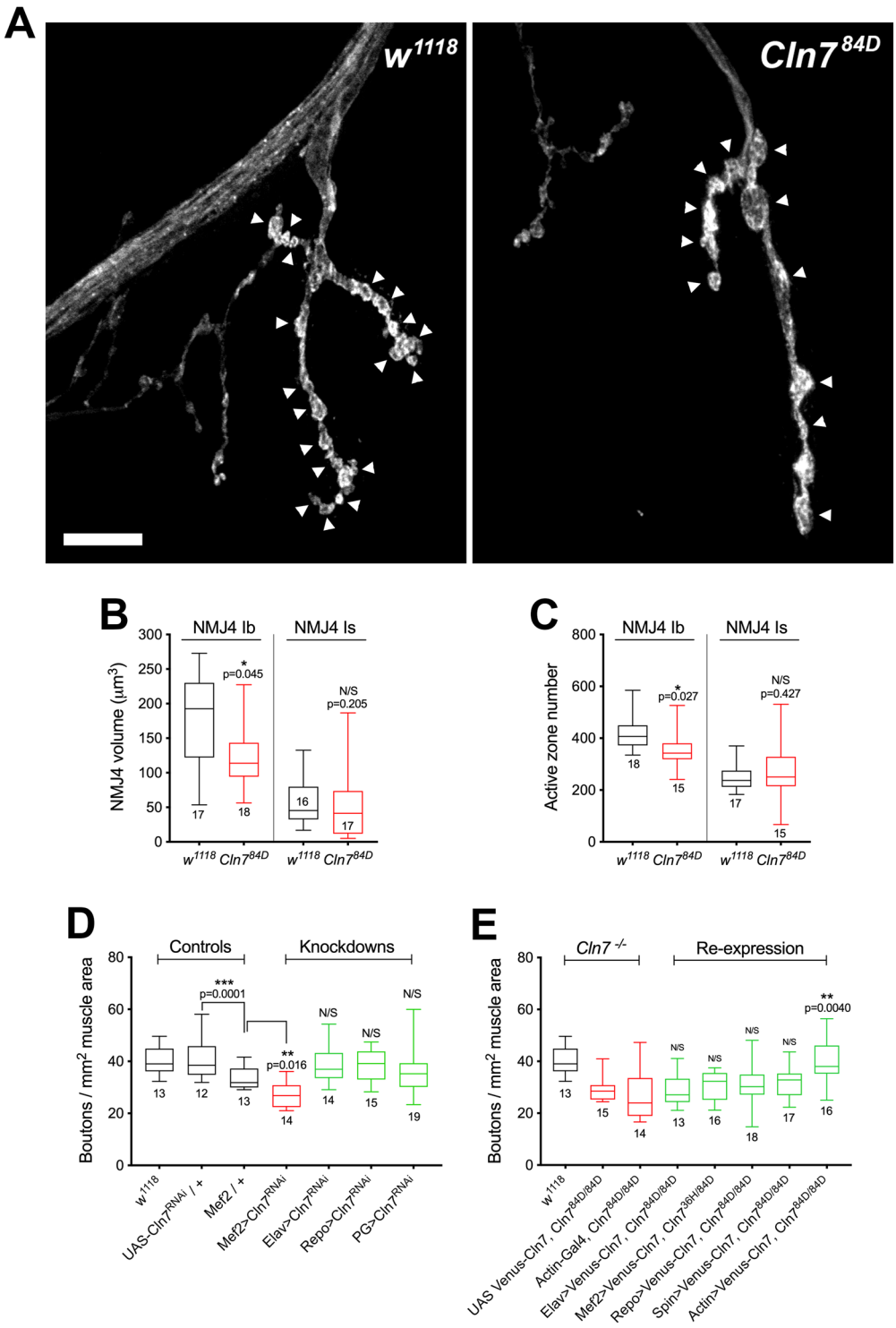

Figure 3. Loss of *Cln7* leads to neurodevelopmental defects. (**A**) Anti-HRP staining of the late larval NMJ of w^{1118} control and $Cln7^{84D}$ flies to visualize the neuronal membrane. Swellings of the pre-synaptic membrane (boutons) are indicated with arrowheads. There are fewer boutons in $Cln7^{84D}$ larvae but these are occasionally swollen. Scale bar = 10 µm. (**B**) The volume of type Ib (I big) junction is reduced in $Cln7^{84D}$ flies but the type Is (I small) junction is unchanged. (**C**) Active zones number is reduced in $Cln7^{84D}$ type Ib but not in type Is junctions. (**B,C**) 2-tailed t-tests, n is indicated). (**D**) The number of boutons can be used as a proxy for junction size. Type Ib junctions are smaller when *Cln7* expression is knocked down post-synaptically in muscle (Mef2-gal4) but not with pre-synaptic (Elav), pan-glial (Repo) or perineurial glial knockdown (PG). (**E**) Normal NMJ development is restored only when *Cln7* is re-expressed ubiquitously (actin-Gal4) in the mutant background. (**D,E**) ANOVA with Dunnett's post-hoc comparisons, n is indicated).

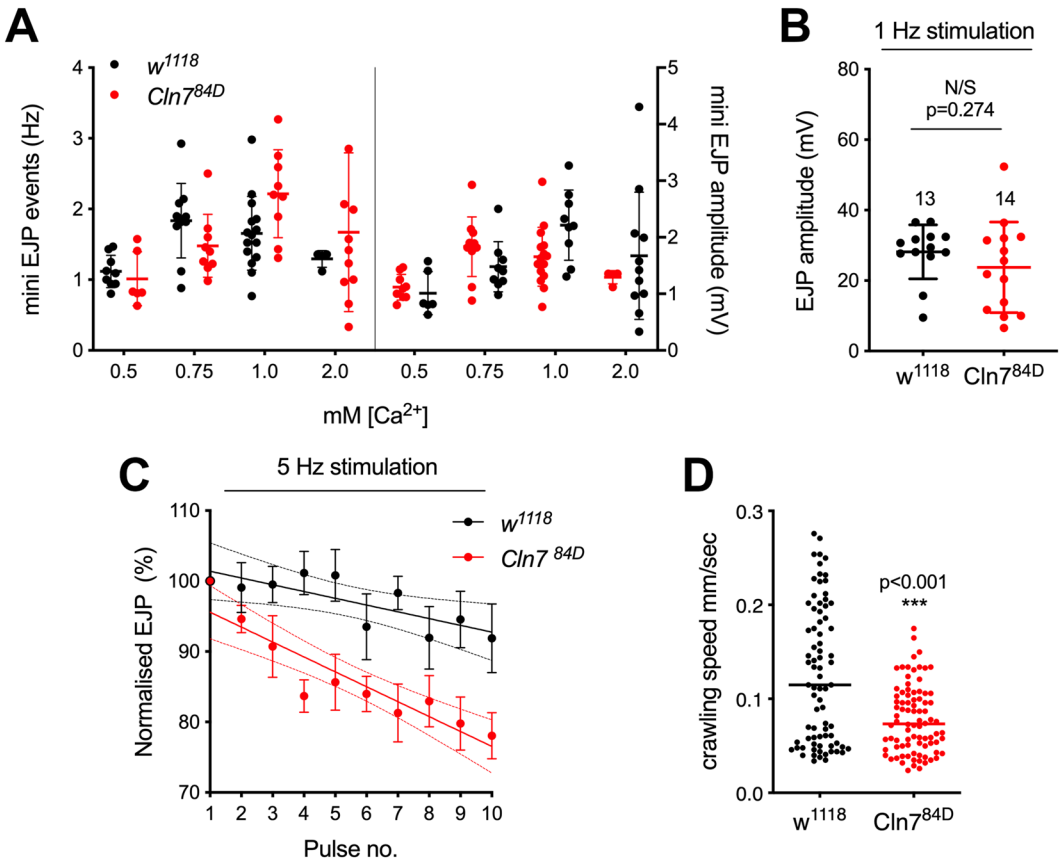

Figure 4. Altered neural function in *Cln7* mutant flies. (**A–C**) Electrophysiological recordings from muscle 4 in w^{1118} control and $Cln7^{84D}$ larvae. (**A**) The frequency (**A**) and amplitude (**B**) of miniature excitatory junction potentials (mEJP) are not significantly changed in *Cln7* larvae. mEJP frequency (left) was calculated over 120 s for each larva and amplitude (right) from 201–835 events using four different concentrations of extracellular Ca^{2+}. Mean is indicated by a solid bar; error bars indicate SD. 2-way ANOVA with Sidak's multiple comparisons. F = 0.6086; DFn = 1; DFd = 66; p = 0.4381 for both. (**B**) Excitatory junction potentials (EJPs) are unchanged in Cln7 larvae. The mean of 16 EJPs at 1 Hz was calculated from n = 13 (w^{1118}) or 14 ($Cln7^{84D}$) in 1 mM Ca^{2+}. Mean is indicated by a solid line; error bars show SD. p = 0.274; Mann-Whitney. (**C**) *Cln7* mutant synapses display an increased rate of fatigue at 5 Hz stimulation. EJP amplitude at 5 Hz was normalized to the mean amplitude at 1 Hz stimulation immediately beforehand. n = 4 NMJs for w^{1118} and =6 for $Cln7^{84D}$. Trend lines fitted by linear regression are shown with solid lines with 95% confidence intervals indicated by dashes. R^2: $w^{1118} = 0.149$; $Cln7^{84D} = 0.383$. The slopes are significantly different: F = 4.786; DFn = 1; DFd = 96; p = 0.0311, t-test. (**D**) Crawling speed is reduced in $Cln7^{84D}$ larvae. Mean speed of w^{1118} control (n = 109) and $Cln7^{84D}$ (n = 86) larvae was determined at 2.5 fps over 5 mins. ****$p < 0.0001$; Mann-Whitney.

Consistent with this, there were no overt changes in the levels of the Glutamate receptors, GluRIIA or GluRIII, in *Cln7* mutant boutons when compared to controls (not shown).

Nerve-evoked excitatory junction potentials (EJPs), were recorded at 1 Hz frequency at 1 mM extracellular Ca^{2+} to evaluate synapse function. We found that EJPs at *Cln7* neuromuscular junctions were similar to those produced by control animals (Fig. 4B). We next applied continuous 5 Hz stimulation to the motor neurons to assess changes in the ability to recruit from the reserve pool of neurotransmitter vesicles. In the control animals, the evoked amplitudes followed a trend towards mild depression as vesicles in the reserve pool become depleted. However, a much more accentuated decline of EJP amplitude was observed in *Cln7* mutant animals under the same conditions (Fig. 4C). This suggests that the reduced synapse size reduces the ability of *Cln7* neurons to activate sufficient vesicles from the reserve pool to deliver a full EJP.

The NMJs regulate body-wall muscle contraction. To identify if the electrophysiological changes we detected led to a quantifiable change in locomotion, we measured instantaneous speed of larval crawling. To address large variations in behavior within a population of larvae, and to avoid the tendency of larvae to avoid open fields, we used a custom 3D printed chamber to record the movement of multiple larvae simultaneously in oval "racetracks" over periods of 5 min (see Methods). *Cln7* mutant larvae move significantly more slowly than isogenic control larvae (Fig. 4D).

Autophagy is unaffected in Cln7 mutants. Defects in the effectiveness of the autophagy pathway are associated with many forms of neurodegenerative disease, including forms of NCL[26] and impairment of autophagy is known to cause a reduction in synapse size similar to that seen in the *Cln7* mutants[21]. In cultured cells,

Cln7 is associated predominantly with lysosomes, which are essential mediators of autophagy and mutations affecting lysosomal function lead to a block in autophagic flux. However, in *Drosophila* normal lysosomal function seems to be critical in the neuron[19,20,27,28], whereas Cln7 is restricted to the post-synaptic partner[16]. Therefore, we asked whether impaired autophagy in the *Cln7* flies might underpin the synaptic phenotypes.

We examined accumulation of p62, a multiple domain protein that acts as a receptor to activate autophagy. Under nutrient-rich conditions, p62 is usually degraded in lysosomes but in starvation conditions autophagic flux is increased and some non-degraded p62 accumulates in lysosomes (Fig. 5A, see w^{1118} control). Thus, p62 levels are often monitored as one readout of autophagic flux. In $Cln7^{84D}$ larvae no p62 accumulates under growth conditions. However, a small but not statistically significant amount of p62 did accumulate under starvation conditions in the $Cln7^{84D}$ larvae, suggesting only a minor impairment in autophagy or lysosomal function (Fig. 5A). This contrasted markedly with *atg18* mutants. Here, p62 clearly accumulated during growth and did so very dramatically under starvation conditions (Fig. 5A). Interestingly, these results are consistent with experiments using *Cln7* deficient cerebellar granule neurons which also failed to show a major defect in autophagy[29].

We also examined whether increasing autophagic flux could rescue the *Cln7* phenotype by inhibiting the TOR complex activity using rapamycin or torin. TORC1 is a central regulator of growth and autophagy and homeostasis in cells and TORC2 is required for normal NMJ development[30]. Inhibition of TORC1 increases autophagic flux which, in the *Drosophila* NMJ, leads to an overgrowth phenotype[21]. Previously, it was reported that inhibiting TORC1 with rapamycin was unable to rescue the smaller NMJ phenotype seen in *atg18* mutants, presumably because autophagy is severely compromised in these animals and this cannot be circumvented[21]. We reasoned that rapamycin treatment would similarly have no effect on the *Cln7* phenotype if it was due to defective autophagy. However, both rapamycin treatment or treatment with the TORC1 and TORC2 inhibitor, torin, caused a robust increase in NMJ size in both control and *Cln7* larvae indicating that autophagic flux can be increased (Fig. 5B). Taken together with the lack of p62 accumulation, and given that autophagy is also not overtly affected in *Cln7* deficient cerebellar granule neurons[29], this suggests that the developmental changes in the *Cln7* animals are not due to defective autophagy.

Normal bone morphogenetic protein (BMP) retrograde signaling in Cln7 mutants. Since Cln7 is required post-synaptically, we examined whether retrograde signaling necessary for normal growth of the pre-synaptic compartment of the NMJ might require Cln7 function. Retrograde signaling allows matching of pre-synapse size and excitability with muscle size; a key retrograde system is based on a BMP-type signal. Glass-bottomed boat (Gbb), a BMP molecule, is secreted from the muscle and binds to the Type I and II receptors Thick veins (Tkv), Saxophone (Sax) and Wishful thinking (Wit) expressed on the neuronal membrane. Ligand binding results in phosphorylation of the SMAD family member Mothers against dpp (Mad) and its retrograde transport to the nucleus. Mutations in *gbb* or the receptors lead to loss of pMad and a smaller NMJ. Conversely, mutations in *Dad*, which encodes an inhibitory SMAD, lead to NMJ synapse overgrowth and a profusion of small, satellite boutons[19,31–33].

Given the enrichment of Cln7 at the PSD and the similarity of the *Cln7* mutant phenotype to those seen for mutations in components of the BMP signaling pathway, we asked whether BMP retrograde signaling is affected by loss of *Cln7*. Potentially Cln7 might act in the post-synaptic muscle cell in the production, processing or presentation of the Gbb ligand. In this case, loss of *Cln7* would give an identical phenotype to loss of Gbb, Tkv, Sax or Wit but a double mutant combination would not make the synapse undergrowth phenotype worse. Similarly, loss of *Cln7* would abolish overgrowth in *Dad* mutants by preventing Mad phosphorylation downstream of Tkv and therefore *Dad;Cln7* double mutants should have a *Cln7*-like undergrowth. We quantified NMJ size in $sax^{4/5}$ and Dad^{J1e4} single mutants and saw the expected undergrowth and overgrowth phenotypes respectively (Fig. 5C). The NMJ synapses size in *sax* mutants was almost identical to the $Cln7^{84D}$ mutants, however, a $sax^{4/5};Cln7^{84D}$ double mutant combination was lethal before late larval stage suggesting an additive effect and indicating that CLN7 and sax operate in different pathways. A $Dad^{J1e4};Cln7^{84D}$ double mutant combination showed a small reduction in overgrowth resulting in an intermediate phenotype. This suggests that phosphorylation of Mad in response to a Gbb signal is intact in the *Cln7* mutant larvae. To further confirm this, we stained the CNS of wild-type and *Cln7* larvae with anti-pMad. The nuclei of motor neurons clearly showed pMad present at the synapse in both genotypes (Fig. 5D).

Loss of Cln7 leads to reduced TORC1 activity in the post-synaptic muscles. TOR complex activity is required for normal homeostatic mechanisms in the nervous system of both *Drosophila* and the mammalian CNS, including retrograde signals emanating from the post-synaptic cell[34–38]. *Cln7* deficient mouse embryonic fibroblasts (MEFs) show a defect in mTORC activation[9] so we considered whether dysregulation of TOR activity might underpin the reduced neural growth in the *Cln7* mutant flies. We stained NMJs with an antibody to phosphorylated S6, which is a marker of TORC1 activity[39]. Phosphorylated S6 was seen clearly to localise at active zones in the pre-synaptic boutons (Fig. 6A). This pattern mirrors the localisation of phosphorylated p70 S6 kinase to active zones reported previously[40] and suggests localised activation of TORC1 at these release sites. The pS6 pattern was retained at active zones in the *Cln7* mutant synapses (Fig. 6A), indicating pre-synaptic TORC1 activity was normal, as expected.

In the post-synaptic muscle cell strong pS6 staining was seen in vesicles that were primarily clustered near the syncitial muscle nuclei and likely to be lysosomes (Fig. 6A; dashed boxes are enlarged to the right, dashed circles in the enlargments show examples of clustered $pS6^{+}$ vesicles). In contrast, the vesicular staining was reduced in the $Cln7^{84D}$ mutant indicating reduced TORC1 activity in absence of Cln7 (Fig. 6A; dashed circles show equivalent peri-nuclear areas). Quantification of the pS6 flourescence intensity in muscles 6 and 7 confirmed a significant reduction in overall intensity in the $Cln7^{84D}$ mutant (Fig. 6B). This is likely to be due to reduced phosphorylation of S6 in muscles rather than a general reduction of S6 as pS6 levels remain unchanged in neurons (Fig. 6B).

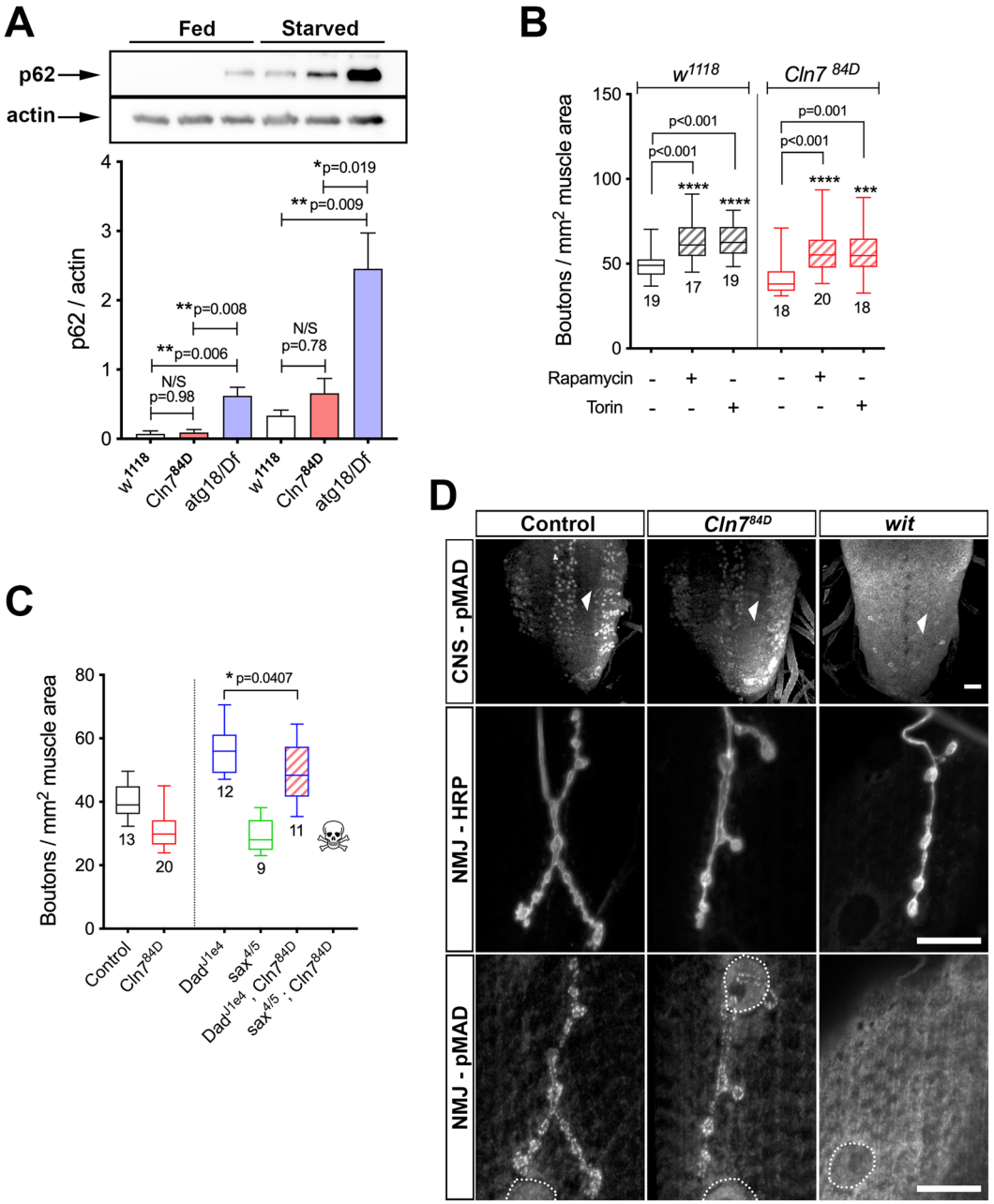

Figure 5. Autophagy and retrograde BMP signaling are unaffected by loss of Cln7. (**A**) The lysosomal substrate, p62, does not accumulate in control of *Cln7*^{84D} larvae when feeding but does in *atg18* mutants. (**A**) After 4 h starvation, p62 accumulates in control animals. Accumulation is slightly but not significantly increased in *Cln7*^{84D} larvae. In contrast, p62 accumulates to very high levels in starved *atg18* mutants. Bars show mean p62 band intensity +/− SEM normalized to actin, n = 3 for each. *p = 0.05; **p < 0.01, ANOVA. (**B**) Inhibition of TORC1 with rapamycin or TORC1 and 2 by torin drives NMJ overgrowth by increasing autophagic flux. *Cln7* mutant larvae respond similarly to control *w*^{1118} larvae suggesting no block in autophagy. ***p = 0.01; ****p < 0.001; ANOVA with Dunnett's post-hoc comparisons, n is indicated. (**C**) Mutations affecting retrograde signaling from the muscle alter neural development. Mutations in the inhibitory SMAD, *Dad*, drive overgrowth of the NMJ; mutations in the *saxophone* type I TGFβ receptor result in underdevelopment at a similar level to *Cln7* mutants. A double *Dad;Cln7* mutant displays a small but significant moderation of the *Dad* phenotype (2-tailed t-test: t = 2.181, Df = 21, p = 0.0407). A *sax;Cln7* double mutant is lethal early in development. Control *w*^{1118} and *Cln7*^{84D} data from Figure 6 are included for comparison. (**D**) Mad is phosphorylated after binding of the Gbb ligand to Tkv, Sax and Wit receptors in the neuron. Characteristic pMad staining is clearly visible in columns of motor neurons in the control and *Cln7*^{84D} CNS but is absent in a *wit* mutant CNS (anti-pMad, top row, arrowheads). pMad staining in boutons is also present in boutons in control and *Cln7*^{84D} NMJs but absent in a *wit* mutant (anti-pMad, bottom column; anti-HRP marks the neuronal plasma membrane, middle column). Similarly, pMad is localized within muscle nuclei but absent in *wit* mutants (dashed circles). Scale bar = 20 μM.

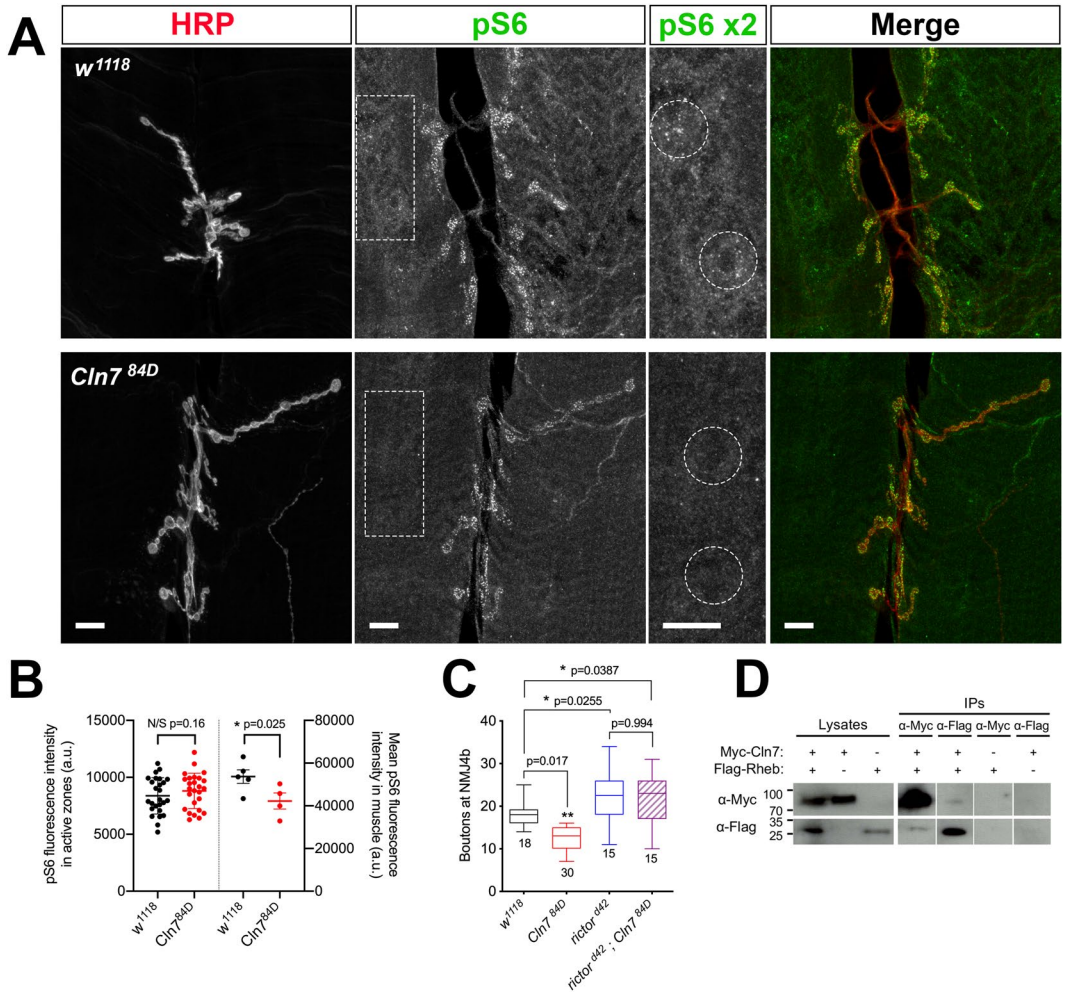

Figure 6. Loss of Cln7 leads to dysregulation of TORC. (**A**) NMJ 6/7 stained for the pre-synaptic membrane (anti-HRP, red) and a marker of TORC1 activity (anti-pS6, green). The RpS6 protein is phosphorylated by TORC1 activity via p70 S6 kinase. Distinct foci of pS6 are present at the active zones in pre-synaptic boutons in both w^{1118} *and* $Cln7^{84D}$ larvae. pS6 staining is prominent in small vesicles in the post-synaptic muscle cell in w^{1118} larvae close to the syncytial muscle nuclei. The $pS6^{+}$ vesicles are largely absent in $Cln7^{84D}$ larvae. Example regions of pS6 staining in the muscle are boxed and enlarged and perinuclear regions circled. Scale bar = 10 μm. (**B**) Quantification of pS6 fluorescence intensity in w^{1118} and $Cln7^{84D}$ larvae. Maximal fluorescence at pre-synaptic active zones at NMJ 6/7 was calculated using plot profile. p = 0.160, one-tailed t-test; n = 26 for both genotypes. Mean fluorescence in the post-synaptic muscles was calculated in 14 square ROIs across muscles 6 and 7 to generate a mean intensity for each animal. p = 0.025, one-tailed t-test; n = 5 for w^{1118} and 4 for $Cln7^{84D}$. (**C**) TORC2 activity is required to restrict pre-synaptic growth. Flies mutant for the TORC2 component, *rictor*, have overgrown type 1b junctions. A *rictor;;Cln7* double mutant also shows an overgrowth phenotype. ANOVA with Dunn's post-hoc comparisons, n is indicated. (**D**) Cln7 can be immunoprecipitated with the TOR complex-activating protein, Rheb. Myc-tagged Cln7 and Flag-tagged Rheb proteins were expressed in *Drosophila* S2 cells.

We next turned to TORC2. TORC2 acts in the neuron to restrict synaptic growth. A mutation in the TORC2-specific subunit, *rictor*, blocks TORC2 activity and leads to a large expansion of the NMJ[30]. We first confirmed the *rictor* mutant phenotype and generated a $rictor^{\Delta 42};Cln7^{84D}$ double mutant. In the double mutant, a similar expansion of the synapse occurred as in the $rictor^{\Delta 42}$ single mutant (Fig. 6C). This places *Cln7* genetically upstream of TORC2 but is consistent with TORC2 functioning principally pre-synaptically in the neuron, downstream of Tsc2[30], with Cln7 acting on the post-synaptic side.

We also identified biochemical evidence linking Cln7 with TORC1. Rheb is a small GTPase that activates mTORC1 in mammalian cells. We expressed epitope-tagged forms of Rheb and Cln7 in *Drosophila* S2 cells and were able to co-immunoprecipiate the two proteins (Fig. 6D), suggesting a molecular interaction between the two. We also find the proteins are colocalised when expressed in *Drosophila* S2 cells (Fig. S2). Taken together, our data indicate that loss of *Cln7* leads to dysregulation of TORC1 activity in the post-synaptic cells. The consequences are developmental changes to the synapse and behavioural changes in the animal.

Discussion

Here we have utilized *Drosophila* as a model system to identify an *in vivo* role for Cln7/MFSD8, the protein whose activity is reduced in late-infantile neuronal ceroid lipofuscinosis, an early onset childhood neurodegenerative disease. The *Drosophila* genome contains orthologues of some but not all the genes associated with neuronal ceroid lipofuscinosis suggesting that, while it may not model all aspects of the disease, it can be used to elucidate the core molecular functions of different NCL genes. We demonstrate that Cln7 is required for normal synaptic development, consistent with a growing appreciation that the synapse is a significant target in neurodegenerative disease. When *Cln7* is disrupted, the *Drosophila* neuromuscular junction fails to reach its normal size having a reduced volume while maintaining normal active zone density. While this is characteristic of mutations affecting autophagic flux within neurons, autophagy is only mildly affected by loss of Cln7. Instead, Cln7 is resident in a vesicular compartment at the post-synaptic side of the junction where it functions to regulate TOR signaling. Previous studies have revealed that TOR signaling has a conserved postsynaptic role to influence retrograde regulation of synaptic activity at central and peripheral synapses in both *Drosophila* and vertebrates[37,38] and that dysregulation of TORC signaling is associated with autism and cognitive decline[41]. Recently it has also been observed that Cln7 is required for TOR reactivation in MEFs[9]. We propose that late-infantile NCL may be a consequence of an early failure of synapse development brought about by dysfunctional TORC signaling.

Lysosome protein function in neural development. Neuronal ceroid lipofuscinosis is a disease with multiple, overlapping forms and with varied ages of onset but which share lysosomal dysfunction as a shared feature. Lysosomal function is essential for autophagic flux and, consistent with a predominantly lysosomal localization for the Cln7 protein in cultured cells, autophagy dysfunction was reported in a Cln7 mutant mouse model[11]. Autophagy is also essential for neural development and long-term neural health, including in *Drosophila*. Given the similarity of the NMJ phenotype in *Cln7* and various *atg* mutants[21], we assumed defective autophagy was likely to be responsible for the *Cln7* phenotypes. However, autophagy appears to be required pre-synaptically in the neuron rather than post-synaptically and, while we cannot rule out a small contribution, we demonstrate here that autophagy is largely intact in the absence of Cln7. Consistent with this, autophagy was also reported to be ostensibly normal in a *Cln7* deficient cerebellar granule neuron cell line[29].

Mutations in other lysosomal genes also affect NMJ development. Two notable examples are *spinster*, which encodes an MFS-domain protein localizing to late endosomes and lysosomes in both neurons and muscle; and *Trpml*, encoding a lysosomal cation channel and homolog of the gene mutated in the human lysosomal storage disorder, mucolipodosis type IV. Loss of *spinster* activity leads to excess reactive oxygen species being generated in the neurons. ROS are a cell-autonomous driver of neural growth in this system[27] and consequently, *spinster* mutants display a large overgrowth of the pre-synaptic compartment[19]. In addition, the retrograde BMP signaling that drives pre-synaptic expansion is also potentiated in the *spinster* mutants, presumably due to inefficient degradation of the active ligand/receptor complex[19]. In *Trpml* mutants, a similar undergrowth of the NMJ occurs to that in *Cln7* mutants[28]. Trpml functions as a Ca^{2+} channel in lysosomes and by regulating an important aspect of lysosomal function – intracellular Ca^{2+} homeostasis – also regulates autophagy and TORC1 activity[20]. However, like Spinster – and in contrast to Cln7 – Trmpl is required pre-synaptically. Here, we demonstrate a post-synaptic specificity for Cln7 that exposes a potential new mechanism dependent on the endo-lysosomal system necessary that regulates synapse size and function in lysosomal storage disorders.

TORC1 and TORC2 activity in neural development. Changes in synapse function have been seen in various models of CLN1 and CLN3 disease and may well be universal to the NCLs e.g.[12,13,42,43]. CNS pathology manifests very early in life in CLN7 disease so it is possible that developmental changes to the CNS and synaptic abnormalities (if also present in human CLN7 disease) predicate for later neuropathology, although potential mechanisms driving this are not yet clear. Might the failure to regulate TOR activity correctly underpin degeneration? The mTORC1 complex has a well-established role regulating neural growth and development in the mammalian nervous system. Several activating mutations upstream of mTORC1, including loss of PTEN or Tsc1/2, result in overgrowth of neurons and increase in density of dendritic spines, as do mutations in the translational repressor, FRMP, downstream of active mTORC1. Consistent with these effects, autism is a highly prevalent co-morbid feature in human disorders caused by mutations in these genes, including tuberous sclerosis, PTEN harmatoma syndrome and Fragile-X syndrome[41]. TORC1 activity also has conserved functions regulating synaptic homeostasis[37,38,44]. The effects of loss of TORC activity on metabolism – particular lipid metabolism – are well recognized[45] but how a reduction in TORC activity effects the nervous system, and how loss might contribute to neurological disease in the NCLs is less well understood. Our identification of molecular interactions between Cln7 and Rheb places Cln7 in the regulatory framework governing TOR activity in neurons but exactly how it functions will require identification of the other Cln7-interacting proteins, the composition of protein complexes involving Cln7 and an understanding of the cargo transported by the Cln7 protein.

Implications for the NCLs. Lysosomal Ca^{2+} homeostasis is affected in several lysosomal disorders, including CLN3 disease[46] and, while Cln7 is not likely to be a Ca^{2+} channel, it will be interesting to ask if changes to Ca^{2+} accompany, and potentially underpin, the loss of post-synaptic TORC activity in Cln7 mutants, as they appear to pre-synaptically in *Trmpl* mutants[20]. Many of the CLN proteins are considered to be lysosomal but lysosomes are predominantly localized in a peri-nuclear location in neurons. However, a proportion of Cln7 also localizes to the plasma membrane in non-polarized, cultured cells[6]. This makes the presence of Cln7 in a vesicular compartment at the post-synaptic membrane intriguing, especially given the co-localization of Cln7 and PSD-95 in the mouse retina[10]. Palmitoyl protein thioesterase (Ppt1) is a lysosomal protease mutated in CLN1 disease. While Ppt1 is clearly lysosomal in most cultured non-neuronal cells, a synaptic pool appears to exist additionally in neurons[47].

Potentially, alternative localizations for the CLN proteins *in vivo* in the CNS may be an important part of the emerging story of synaptic dysfunction in the NCLs.

Materials and Methods

Drosophila lines. *Drosophila* lines were obtained from the Bloomington Stock Center at Indiana University except for an isogenic w^{1118} control strain from the Vienna *Drosophila* Resource Center; PG-Gal4 (*NP6293) from the Kyoto DGRC Stock Center*; Spin-Gal4 and Dad^{j1e4} from Dr. Sean Sweeney (University of York, UK); and $rictor^{\Delta 42}$ from Dr. Joseph Bateman (King's College London). Gal4 lines used with stock numbers as of January 2019 were as follows: actin (BL3954); $Elav^{c155}$ (BL458); Mef2 (BL27930); vGlut (BL26160); Repo (BL7415); PG (Kyoto: 105188). The Cln7 RNAi line used was yv;TRiP.HMC03819 (BL55664). To generate UAS-Venus-Cln7, the full-length Cln7 ORF was amplified by proofreading PCR using clone GH22722 as a template and cloned into pENTR/D-Topo. After sequence verification it was recombined into the pTVW destination vector obtained from the *Drosophila* Genetics Resource Center, University of Indiana and transformants generated by BestGene.

Generation of *Cln7* mutants. The P-element NP0345 inserted in the 5′UTR of the *Cln7* locus (CG8596) was excised by mating to the Δ2–3 transposase line. Two independent deletion alleles, 36H and 84D, were identified by PCR and subsequently backcrossed over 6 generations to the isogenic w^{1118} control.

Visualization of the larval NMJ. The pre-synaptic membrane was visualized with Alexa-594 goat anti-HRP (1;1000; Jackson Immuno) except for volume measurements from confocal z-sections when a membrane-localized GFP was used (OK371-Gal4, UAS-CD8::GFP) with rabbit anti-GFP (AbCam ab290, 1:1000). To ensure constant culture density and conditions between samples, cohorts of 100 1st instar larvae were picked from the agar plates and transferred to vials of freshly made food and incubated for 3–4 days until wandering 3rd instar stage. Larval flat mounts were immunostained using standard procedures. Briefly, tissue was fixed for 20 min in 4% EM-grade formaldehyde in HL-3. After washing, tissue was permeabilised and blocked in 1% BSA, 0.3% Triton X-100 in PBS. Antibodies were diluted in blocking solution and incubated overnight at 4 °C for primary antibodies and for 2 h at room temperature for secondary antibodies. Stained tissue was mounted in Prolong Gold and visualized on a Zeiss LSM510 Meta, LSM780 or LSM880 Airsycan confocal microscopes using 40X N.A. 1.4 oil immersion, 40X N.A. 1.2 water immersion or 100x N.A. 1.46 oil immersion PlanApo lenses, respectively. Active zones were stained with mouse anti-Bruchpilot (clone NC82, 1:25; Developmental Studies Hybridoma Bank) and the post-synaptic density with anti-Dlg (clone 4F3, 1:20; DSHB). Rabbit anti-pMAD (1:500) was a gift of Prof. Carl-Henrik Heldin (Ludwig Institute for Cancer Research, Uppsala). YFP-Cln7 was visualized with rabbit anti-GFP (1:5000; AbCam ab290). Rabbit anti-pS6 (1:400) was a gift of Dr. Jongkyeong Chung, Seoul National University[39]. Alexa-488 and Alexa-594-conjugated secondary antibodies were from Jackson Immuno Research and used at 1:500 dilution.

Quantification of NMJ size. Volumes were acquired with an optical slice width of 1.0 μM and steps of 0.5 μM using a 40x N.A. 1.4 PlanApo objective and zoom = 2.0. Volocity was used to render the volumes then to measure the volume of the pre-synaptic membrane and to count active zones. Boutons were counted manually for the type Ib junction on muscle 4 of segments A3-A5. In each case a transmitted light image of the corresponding muscle was obtained at 10x and the muscle surface area calculated by outlining in ImageJ. Bouton number was then normalized to the muscle surface area.

Quantification of pS6 fluorescence. pS6 fluorescence was quantified from single optical planes collected using a 25x N.A. 0.8 water immersion objective. The mean fluorescence from square ROIs of area 185 μm^2 of muscles 6 and 7 was calculated in imageJ, avoiding trachea and bright pre-synaptic puncta. The mean of the 14 areas was used as the mean fluorescent intensity for that animal. The plot profile tool was used to report the maximal fluorescence of individual active zones.

Quantification of larval movement. Wandering 3rd instar stage larvae were transferred to a custom 3D-printed chamber comprising 12 oval troughs each 3 mm deep and with a track length of 75 mm. Each trough was lined with a thin coating of 3% w/v agar. The chamber was lit from below by a LED light table and filmed from above with a Basler GigE camera. Cohorts of 12 larvae crawling were filmed for 5 min each and their position tracked at 2.5 fps using Ethovision software.

Electrophysiology. Wandering 3rd instar larvae were dissected in HL3.1 supplemented with Ca^{2+} concentration at 0.5, 0.75, 1.0 or 2.0 mM depending on the paradigm[48]. Recordings were made from muscle 4 of segments A3-A5 using standard protocols[49]. Baseline synaptic transmission was characterized by recording mEJPs for 2 min and 16 EJPs stimulated at 1 Hz. For high frequency stimulation, 16 EPSPs at 1 Hz were recorded followed by 5 Hz stimulation for 5 min. In all experiments a minimum of 8 larvae were used with maximum of 2 recordings per larva. In each case the starting resting potential of the muscle was −60 to −75 mV and resistance of 5–10 mΩ. Analysis of electrophysiological recordings was performed in Clampfit 10.0 and data exported for further analysis in Prism 7.0.

***Drosophila* starvation assay.** First instar larvae of control w^{1118}, $Cln7^{84D}$ and $atg18a^{KG03090}$/Df(3 L)Exel6112 were transferred in cohorts of 20 from grape juice agar plates to standard food vials smeared with fresh yeast paste and allowed to develop for a further 24 h at 25 °C. Larvae were then removed from the food and protein samples prepared for each genotype. The remaining 10 larvae for each genotype were starved of amino acids for 4 h at 25 °C. Lysates of total protein were prepared by manually crushing the larvae with a mini-pestle directly into 200 μl Laemmli buffer containing 8 mM DTT and protease inhibitors.

Cell transfection, immunoprecipitation and immunofluorescence. To generate expression plasmids, the *Cln7* pENTR clone was recombined into pAMW. The full-length Rheb ORF was amplified from clone GH10361 and cloned in to pENTR. After sequence verification it was recombined in pAFW. Tagged proteins were immunoprecipitated with Myc-Trap_MA beads or anti-FLAG M2 Affinity gel overnight at 4 °C. For immunofluorescence, cells were fixed 48 h after transfection in 4% formaldehyde in PBS for 10 min then stained as for larval tissue except that Hoechst was added to the diluted secondary antibodies at 1:10,000 to label DNA. Coverslips were mounted in ProLong Gold (Thermo) and viewed on a LSM780 confocal microscope. Primary mouse anti-Flag and goat anti-myc were the same as for western blots but used at 1:500. Secondary antibodies were Alexa-488 donkey anti-goat and Alexa-594 donkey anti-mouse (1:500; Jackson Immuno Research).

Western blotting. Protein were separated by standard SDS-PAGE and transferred to PVDF membranes by wet transfer. Primary antibodies were: mouse anti-Flag M2 (1:5000; Sigma); goat anti-myc (1:1000; AbCam ab9132); rabbit anti-Ref(2)P (*Drosophila* homologue of p62, 1:500; a gift of Dr. Gabor Juhasz, Eötvös Loránd University, Budapest); and mouse anti-actin (clone JLA-20, 1:500; DSHB). Secondary antibodies were HRP-conjugated goat anti-mouse or anti-rabbit IgG (both 1:4000, Cell Signaling Technologies). Detection of HRP was with SuperSignal West Femto ECL reagent in conjunction with a Vilber Fusion FX system. p62 levels were normalized to actin from 16-bit images using ImageJ.

Statistical analysis. All statistical tests were performed within Prism 7. Normality of datasets was determined using a D'Agostino-Pearson test and datasets not conforming to Gaussian distributions were transformed with logarithmic or reciprocal transformations. Non-parametric tests were used where distributions remained non-Gaussian after transformation. Survival was compared by log-rank analysis. Samples sizes and tests used are described in the figure legends. Significance in all cases was set at $p < 0.05$.

Received: 26 July 2019; Accepted: 3 October 2019;
Published online: 30 October 2019

References

1. Jalanko, A. & Braulke, T. Neuronal ceroid lipofuscinoses. *Biochim Biophys Acta* **1793**, 697–709, https://doi.org/10.1016/j.bbamcr.2008.11.004 (2009).
2. Kielar, C. *et al*. Molecular correlates of axonal and synaptic pathology in mouse models of Batten disease. *Hum Mol Genet* **18**, 4066–4080, https://doi.org/10.1093/hmg/ddp355 (2009).
3. Koch, S. *et al*. Morphologic and functional correlates of synaptic pathology in the cathepsin D knockout mouse model of congenital neuronal ceroid lipofuscinosis. *J Neuropathol Exp Neurol* **70**, 1089–1096, https://doi.org/10.1097/NEN.0b013e318238fc28 (2011).
4. Kousi, M. *et al*. Mutations in CLN7/MFSD8 are a common cause of variant late-infantile neuronal ceroid lipofuscinosis. *Brain* **132**, 810–819, https://doi.org/10.1093/brain/awn366 (2009).
5. Siintola, E. *et al*. The novel neuronal ceroid lipofuscinosis gene MFSD8 encodes a putative lysosomal transporter. *Am J Hum Genet* **81**, 136–146, https://doi.org/10.1086/518902 (2007).
6. Steenhuis, P., Herder, S., Gelis, S., Braulke, T. & Storch, S. Lysosomal targeting of the CLN7 membrane glycoprotein and transport via the plasma membrane require a dileucine motif. *Traffic* **11**, 987–1000, https://doi.org/10.1111/j.1600-0854.2010.01073.x (2010).
7. Sharifi, A. *et al*. Expression and lysosomal targeting of CLN7, a major facilitator superfamily transporter associated with variant late-infantile neuronal ceroid lipofuscinosis. *Hum Mol Genet* **19**, 4497–4514, https://doi.org/10.1093/hmg/ddq381 (2010).
8. Chapel, A. *et al*. An extended proteome map of the lysosomal membrane reveals novel potential transporters. *Mol Cell Proteomics* **12**, 1572–1588, https://doi.org/10.1074/mcp.M112.021980 (2013).
9. Danyukova, T. *et al*. Loss of CLN7 results in depletion of soluble lysosomal proteins and impaired mTOR reactivation. *Hum Mol Genet* **27**, 1711–1722, https://doi.org/10.1093/hmg/ddy076 (2018).
10. Khan, K. N. *et al*. Specific Alleles of CLN7/MFSD8, a Protein That Localizes to Photoreceptor Synaptic Terminals, Cause a Spectrum of Nonsyndromic Retinal Dystrophy. *Invest Ophthalmol Vis Sci* **58**, 2906–2914, https://doi.org/10.1167/iovs.16-20608 (2017).
11. Brandenstein, L., Schweizer, M., Sedlacik, J., Fiehler, J. & Storch, S. Lysosomal dysfunction and impaired autophagy in a novel mouse model deficient for the lysosomal membrane protein Cln7. *Hum Mol Genet* **25**, 777–791, https://doi.org/10.1093/hmg/ddv615 (2016).
12. Aby, E. *et al*. Mutations in palmitoyl-protein thioesterase 1 alter exocytosis and endocytosis at synapses in Drosophila larvae. *Fly (Austin)* **7**, 267–279, https://doi.org/10.4161/fly.26630 (2013).
13. Grunewald, B. *et al*. Defective synaptic transmission causes disease signs in a mouse model of juvenile neuronal ceroid lipofuscinosis. *Elife* **6**, https://doi.org/10.7554/eLife.28685 (2017).
14. Charng, W. L., Yamamoto, S. & Bellen, H. J. Shared mechanisms between Drosophila peripheral nervous system development and human neurodegenerative diseases. *Curr Opin Neurobiol* **27**, 158–164, https://doi.org/10.1016/j.conb.2014.03.001 (2014).
15. Muzaffar, N. E. & Pearce, D. A. Analysis of NCL Proteins from an Evolutionary Standpoint. *Curr Genomics* **9**, 115–136, https://doi.org/10.2174/138920208784139573 (2008).
16. Mohammed, A., O'Hare, M. B., Warley, A., Tear, G. & Tuxworth, R. I. *In vivo* localization of the neuronal ceroid lipofuscinosis proteins, CLN3 and CLN7, at endogenous expression levels. *Neurobiol Dis* **103**, 123–132, https://doi.org/10.1016/j.nbd.2017.03.015 (2017).
17. Menon, K. P., Carrillo, R. A. & Zinn, K. Development and plasticity of the Drosophila larval neuromuscular junction. *Wiley Interdiscip Rev Dev Biol* **2**, 647–670, https://doi.org/10.1002/wdev.108 (2013).
18. Frank, C. A. Homeostatic plasticity at the Drosophila neuromuscular junction. *Neuropharmacology* **78**, 63–74, https://doi.org/10.1016/j.neuropharm.2013.06.015 (2014).
19. Sweeney, S. T. & Davis, G. W. Unrestricted synaptic growth in spinster-a late endosomal protein implicated in TGF-beta-mediated synaptic growth regulation. *Neuron* **36**, 403–416 (2002).
20. Wong, C. O., Li, R., Montell, C. & Venkatachalam, K. Drosophila TRPML is required for TORC1 activation. *Curr Biol* **22**, 1616–1621, https://doi.org/10.1016/j.cub.2012.06.055 (2012).
21. Shen, W. & Ganetzky, B. Autophagy promotes synapse development in Drosophila. *J Cell Biol* **187**, 71–79, https://doi.org/10.1083/jcb.200907109 (2009).
22. Faller, K. M. *et al*. The neuronal ceroid lipofuscinoses: Opportunities from model systems. *Biochim Biophys Acta* **1852**, 2267–2278, https://doi.org/10.1016/j.bbadis.2015.04.022 (2015).
23. Mayfield, J. D. & Ward, D. N. Effects of clomiphene on ovarian ascorbic acid and the response to luteinizing hormone. *Acta Endocrinol (Copenh)* **51**, 557–562, https://doi.org/10.1530/acta.0.0510557 (1966).

24. Lnenicka, G. A. & Keshishian, H. Identified motor terminals in Drosophila larvae show distinct differences in morphology and physiology. *J Neurobiol* **43**, 186–197 (2000).
25. Wagh, D. A. *et al*. Bruchpilot, a protein with homology to ELKS/CAST, is required for structural integrity and function of synaptic active zones in Drosophila. *Neuron* **49**, 833–844, https://doi.org/10.1016/j.neuron.2006.02.008 (2006).
26. Seranova, E. *et al*. Dysregulation of autophagy as a common mechanism in lysosomal storage diseases. *Essays Biochem* **61**, 733–749, https://doi.org/10.1042/EBC20170055 (2017).
27. Milton, V. J. *et al*. Oxidative stress induces overgrowth of the Drosophila neuromuscular junction. *Proc Natl Acad Sci USA* **108**, 17521–17526, https://doi.org/10.1073/pnas.1014511108 (2011).
28. Wong, C. O. *et al*. A TRPV channel in Drosophila motor neurons regulates presynaptic resting Ca2+ levels, synapse growth, and synaptic transmission. *Neuron* **84**, 764–777, https://doi.org/10.1016/j.neuron.2014.09.030 (2014).
29. von Kleist, L. *et al*. A newly generated neuronal cell model of CLN7 disease reveals aberrant lysosome motility and impaired cell survival. *Mol Genet Metab*. https://doi.org/10.1016/j.ymgme.2018.09.009 (2018).
30. Natarajan, R., Trivedi-Vyas, D. & Wairkar, Y. P. Tuberous sclerosis complex regulates Drosophila neuromuscular junction growth via the TORC2/Akt pathway. *Hum Mol Genet* **22**, 2010–2023, https://doi.org/10.1093/hmg/ddt053 (2013).
31. Aberle, H. *et al*. wishful thinking encodes a BMP type II receptor that regulates synaptic growth in Drosophila. *Neuron* **33**, 545–558 (2002).
32. McCabe, B. D. *et al*. The BMP homolog Gbb provides a retrograde signal that regulates synaptic growth at the Drosophila neuromuscular junction. *Neuron* **39**, 241–254 (2003).
33. Rawson, J. M., Lee, M., Kennedy, E. L. & Selleck, S. B. Drosophila neuromuscular synapse assembly and function require the TGF-beta type I receptor saxophone and the transcription factor Mad. *J Neurobiol* **55**, 134–150, https://doi.org/10.1002/neu.10189 (2003).
34. Henry, F. E. *et al*. Retrograde changes in presynaptic function driven by dendritic mTORC1. *J Neurosci* **32**, 17128–17142, https://doi.org/10.1523/JNEUROSCI.2149-12.2012 (2012).
35. Tang, S. J. *et al*. A rapamycin-sensitive signaling pathway contributes to long-term synaptic plasticity in the hippocampus. *Proc Natl Acad Sci USA* **99**, 467–472, https://doi.org/10.1073/pnas.012605299 (2002).
36. Hou, L. & Klann, E. Activation of the phosphoinositide 3-kinase-Akt-mammalian target of rapamycin signaling pathway is required for metabotropic glutamate receptor-dependent long-term depression. *J Neurosci* **24**, 6352–6361, https://doi.org/10.1523/JNEUROSCI.0995-04.2004 (2004).
37. Penney, J. *et al*. TOR is required for the retrograde regulation of synaptic homeostasis at the Drosophila neuromuscular junction. *Neuron* **74**, 166–178, https://doi.org/10.1016/j.neuron.2012.01.030 (2012).
38. Henry, F. E. *et al*. A Unique Homeostatic Signaling Pathway Links Synaptic Inactivity to Postsynaptic mTORC1. *J Neurosci* **38**, 2207–2225, https://doi.org/10.1523/JNEUROSCI.1843-17.2017 (2018).
39. Kim, W., Jang, Y. G., Yang, J. & Chung, J. Spatial Activation of TORC1 Is Regulated by Hedgehog and E2F1 Signaling in the Drosophila Eye. *Dev Cell* **42**, 363–375 e364, https://doi.org/10.1016/j.devcel.2017.07.020 (2017).
40. Cheng, L., Locke, C. & Davis, G. W. S6 kinase localizes to the presynaptic active zone and functions with PDK1 to control synapse development. *J Cell Biol* **194**, 921–935, https://doi.org/10.1083/jcb.201101042 (2011).
41. Lipton, J. O. & Sahin, M. The neurology of mTOR. *Neuron* **84**, 275–291, https://doi.org/10.1016/j.neuron.2014.09.034 (2014).
42. Kim, S. J. *et al*. Palmitoyl protein thioesterase-1 deficiency impairs synaptic vesicle recycling at nerve terminals, contributing to neuropathology in humans and mice. *J Clin Invest* **118**, 3075–3086, https://doi.org/10.1172/JCI33482 (2008).
43. Llavero Hurtado, M. *et al*. Proteomic mapping of differentially vulnerable pre-synaptic populations identifies regulators of neuronal stability *in vivo*. *Sci Rep* **7**, 12412, https://doi.org/10.1038/s41598-017-12603-0 (2017).
44. Bateup, H. S. *et al*. Excitatory/inhibitory synaptic imbalance leads to hippocampal hyperexcitability in mouse models of tuberous sclerosis. *Neuron* **78**, 510–522, https://doi.org/10.1016/j.neuron.2013.03.017 (2013).
45. Howell, J. J. & Manning, B. D. mTOR couples cellular nutrient sensing to organismal metabolic homeostasis. *Trends Endocrinol Metab* **22**, 94–102, https://doi.org/10.1016/j.tem.2010.12.003 (2011).
46. Chandrachud, U. *et al*. Unbiased Cell-based Screening in a Neuronal Cell Model of Batten Disease Highlights an Interaction between Ca2+ Homeostasis, Autophagy, and CLN3 Protein Function. *J Biol Chem* **290**, 14361–14380, https://doi.org/10.1074/jbc.M114.621706 (2015).
47. Ahtiainen, L., Van Diggelen, O. P., Jalanko, A. & Kopra, O. Palmitoyl protein thioesterase 1 is targeted to the axons in neurons. *J Comp Neurol* **455**, 368–377, https://doi.org/10.1002/cne.10492 (2003).
48. Stewart, B. A., Atwood, H. L., Renger, J. J., Wang, J. & Wu, C. F. Improved stability of Drosophila larval neuromuscular preparations in haemolymph-like physiological solutions. *J Comp Physiol A* **175**, 179–191 (1994).
49. Zhang, B. & Stewart, B. Electrophysiological recording from Drosophila larval body-wall muscles. *Cold Spring Harb Protoc* **2010**, pdb prot5487, https://doi.org/10.1101/pdb.prot5487 (2010).

Acknowledgements

The authors are very grateful to Drs. Sean Sweeney and Joe Bateman for sending *Drosophila* lines; and to Dr. Gabor Juhasz, Prof. Carl-Henrik Heldin and Dr. Jongkyeong Chung for the anti-Ref(2)P, anti-pMad and anti-pS6 antibodies, respectively. Research was funded by The Wellcome Trust grant number 082004 to GT and by a Biotechnology and Biological Sciences Research Council New Investigator award BB/N008472/1 to RIT. BAS was supported by a Natural Sciences and Engineering Research Council of Canada grant number 250078. MO'H was supported by a King's College, London Quota BBSRC PhD studentship and a KCL Peter Baker Travelling Fellowship.

Author contributions

M.B.O'H. generated the *Cln7* mutant lines. K.J.C., M.B.O'H., A.M., K.M.A., N.C.A., M.J.T. and R.I.T. analyzed the mutant phenotypes. K.J.C. performed the interaction experiments. K.M.A. and R.I.T. designed and analyzed the larval crawling assay. M.B.O'H. and B.A.S. performed the electrophysiological study and analyzed the data. R.I.T. and G.T. conceived of and supervised the study. R.I.T. and G.T. wrote the manuscript.

Competing interests

The authors declare no competing interests.

Additional information

Supplementary information is available for this paper at https://doi.org/10.1038/s41598-019-51588-w.

Correspondence and requests for materials should be addressed to R.I.T. or G.T.

Reprints and permissions information is available at www.nature.com/reprints.